ChemPhysChem

Research Article
doi.org/10.1002/cphc.202300467

Chemistry Europe
European Chemical Societies Publishing

www.chemphyschem.org

Special Issue

Temperature-Dependent Line-Broadening Effects in CO_2 Caused by Ar

Jamel Salem,*[a] Roland Tóbiás,[b] Attila G. Császár,*[b, c] Muneerah Mogren Al-Mogren,[d] Nejm-Edine Jaidane,[e] and Majdi Hochlaf*[f]

This computational study of line-broadening effects is based on an accurate, analytical representation of the intermonomer potential energy surface (PES) of the CO_2·Ar van der Waals (vdW) complex. The PES is employed to compute collisional broadening coefficients for rovibrational lines of CO_2 perturbed by Ar. The semiclassical computations are performed using the modified Robert–Bonamy approach, including real and imaginary terms, and the exact trajectory model. The lines investigated are in the 10001←00011, 01101←00001, 00011←00001, and 00031←00001 vibrational bands and the computations are repeated at multiple temperatures. The computed results are in good agreement with the available experimental values, validating both the intermonomer PES developed and the methodology used. For lines in the 01101←00001 band of CO_2, temperature-dependent Ar-broadening coefficients are reported for the first time. The parameters presented should prove useful, among other applications, for the accurate experimental determination of CO_2 and Ar abundances in planetary atmospheres.

Introduction

Carbon dioxide, CO_2, is a dominant species in the atmospheres of Venus and Mars and it is the fourth most abundant molecule in the Earth's atmosphere. Thus, CO_2 is an important contributor to the greenhouse effect and its significant impact on the radiative balance of atmospheres becomes especially relevant when environmental and climate-change effects are examined in dry atmospheres. The accurate determination of CO_2 abundances and their vertical distributions becomes particularly important when better understanding of the physical and chemical processes occurring in planetary atmospheres is seeked. Accurate retrieval of abundances requires detailed simulation of CO_2 rovibrational bands under diverse measurement conditions. Like for all the other molecules present in atmospheres, the rovibrational lines of CO_2 are subject to temperature-dependent collisional broadening and shifting. Therefore, measurement and computation of line-shape changes induced by different perturbers have special significance.

Most of the early spectroscopic measurements of broadenings and shiftings of CO_2 lines were not accompanied by accurate first-principles computations. This has changed with the development of dependable models and efficient computational strategies. The theoretical models employed highlighted the importance of the accurate treatment of intermolecular interactions, including the appropriate consideration of the intricate and noticeably anisotropic interactions between CO_2 and the perturber. The type of collider considered affects significantly and mostly unpredictably, at least in a quantitative sense, these interactions and their spectral effects. The collision-induced changes in the rovibrational lines of CO_2 caused by a rare-gas (Rg) atom are closely connected with the translational velocity of Rg. As a result, the exact trajectory model proposed by Buldyreva and co-workers[1,2] represents an improvement over the parabolic trajectory used within the Robert–Bonamy (RB) formalism.[3] This model should be used with a high-quality potential energy surface (PES), describing the CO_2–Rg intermonomer interactions as accurately as feasible.

[a] Dr. J. Salem
Université de Gafsa, Laboratoire Technologie, Energie (Matériaux Innovants, Faculté des Sciences, Sidi Ahmed Zarroug – 2112 Gafsa, Tunisia
E-mail: sfjamel1@yahoo.fr

[b] Dr. R. Tóbiás, Prof. Dr. A. G. Császár
Laboratory of Molecular Structure and Dynamics, Institute of Chemistry, ELTE Eötvös Loránd University, Pázmány Péter sétány 1/A, H-1117 Budapest, Hungary
E-mail: attila.csaszar@ttk.elte.hu

[c] Prof. Dr. A. G. Császár
HUN-REN–ELTE Complex Chemical Systems Research Group, H-1518 Budapest 112, P.O. Box 32, Hungary
E-mail: attila.csaszar@ttk.elte.hu

[d] Dr. M. Mogren Al-Mogren
Department of Chemistry, College of Sciences, King Saud University, P.O. Box 2455, Riyadh 11451, Saudi Arabia

[e] Prof. Dr. N.-E. Jaidane
Laboratoire de Spectroscopie Atomique, Moléculaire et Applications LSAMA, Université de Tunis Al Manar, Tunis, Tunisia

[f] Prof. Dr. M. Hochlaf
Université Gustave Eiffel, COSYS/IMSE, 5 Bd Descartes, 77454 Champs sur Marne, France
E-mail: majdi.hochlaf@univ-eiffel.fr

Supporting information for this article is available on the WWW under https://doi.org/10.1002/cphc.202300467

Special Issue An invited contribution to a Special Collection dedicated to Pablo Villarreal Herrán on the occasion of his 70th birthday

In this study, we are investigating the broadening, but not the shifting, of lines in certain CO_2 bands caused by the binary collision of a CO_2 molecule with an Ar atom. In the Earth's atmosphere, Ar is the third most abundant gas after N_2 and O_2, with close to 1% abundance. Thus, collisions between CO_2 and Ar contribute significantly to the broadening of CO_2 lines. Furthermore, these collisions have an impact on the radiative balance of the Earth's atmosphere. Understanding the role of CO_2 in the radiative balance motivated several experimental, theoretical, and computational studies, with investigations over a wide range of pressure and temperature values.[4–20] It is worth reiterating some of the most important results.

In 1974, the line widths of Ar-broadened CO_2 transitions have been determined by Boulet *et al.*[4] in the 10001←00011 band, utilizing a stable laser source. These measurements were carried out for both the P and R branches at 300 K, with an average uncertainty of 6.7×10^{-3} $cm^{-1}atm^{-1}$. In 1992, Thibaut *et al.*[5] used a Fourier-transform (FT) spectrometer and looked at the rovibrational lines of the 00031←00001 band of CO_2 in an Ar buffer gas, again at room temperature, and deduced collisional broadening coefficients of CO_2 lines after fitting the experimental spectra with a Voigt profile. In 2001, a combined experimental and computational investigation was performed, again by Thibault and co-workers,[6] targeting the broadening of lines in the 00011←00001 band of CO_2 perturbed by Ar at various temperatures. This study utilized infrared FT spectroscopy, quantum-mechanical close-coupling and coupled-states approaches, as well as improved Smith–Giraud–Cooper and Robert–Bonamy methods. In the same year, semiclassical calculations were performed,[7] in the temperature range of 160–760 K, for lines of the 00011←00001 band broadened by Ar. Buldyreva and Chrysos[7] worked within the framework of the RB approach improved by the exact trajectory model. These computations utilized an old PES for the weakly bound complex $CO_2\cdot$Ar, computed by Parker and co-workers.[21] Comparison of the computed data with the available experimental results showed good agreement, validating the RB approach combined with the exact trajectory model.

In recent years, collision-induced broadening of lines in the 00011←00001 and 00031←00001 bands have been studied further. For example, Cole *et al.*[16] reinvestigated the 00031←00001 band using dual frequency comb absorption and phase spectroscopy up to 25 bar and 1000 K, while Chen *et al.*[18] applied tunable diode laser absorption spectroscopy for transitions with high J values, where J is the quantum number characterizing the overall rotation of the molecule. Furthermore, Arshinov and co-workers[22–24] utilized a frequency-stabilized CO_2 laser to probe the unsaturated absorption coefficients of lines in the 10001←00011 band in pure CO_2, as well as in binary mixtures of CO_2 with various gases, including Ar, in the temperature range of 296–700 K.

In contrast to the 00011←00001 and 00031←00001 bands, the 01101←00001 band of CO_2, despite its considerable importance in the context of the greenhouse effect, was examined only to a moderate extent: the literature is limited to collision-induced self-, N_2-, and O_2-broadening values.[25–29] To the best of our knowledge, Ar-broadenings of lines in the 01101←00001 band have not been considered in the literature.

To determine the line-broadening parameters of CO_2 colliding with Ar, an accurate PES for the weakly-bound $CO_2\cdot$Ar complex must be generated. It is mandatory to obtain an accurate description of the long-range interactions, as this becomes particularly important when modeling the pressure effect. One needs an analytical expression for the PES, which must then be incorporated into a code computing line-broadening parameters. In this study, an accurate interaction PES is built and the Ar-broadening parameters are obtained within a semiclassical framework. Comparison of our results with the available experimental determinations reveals good agreement, improved over earlier theoretical data for lines in the 00011←00001, 10001←00011, and 00031←00001 bands. This study provides, for the first time, Ar-broadenings for transitions of the 01101←00001 band. These data should prove useful for applications in planetary, astrophysical, and chemical sciences.

The structure of this paper is as follows. The next section details how the PES of the $CO_2\cdot$Ar vdW complex utilized for the scattering computations was generated. The following section describes the steps involved in the determination of line widths and their temperature dependence. Next, we discuss our results for lines in the 10001←00011, 00031←00001, 00011←00001, and 01101←00001 bands of CO_2. The closing section of the paper summarizes the principal findings of this study.

Potential Energy Surface of the $CO_2\cdot$Ar Interacting System

It is widely appreciated that computed line-broadening coefficients, particularly for molecules formed by strong covalent bonds, like CO_2, depend only very slightly on the intramolecular degrees of freedom. It is also true that by now there are codes available, like autoPES,[30,31] which make the production of high-quality interaction PESs based on high-level electronic-structure computations almost automatic.

The actual computation of line-broadening effects must be carried out using simple prescribed functional forms. This means that the PES we are going to utilize in this study was generated in two steps. First, a four-dimensional (4D) PES was built with the code autoPES, which was then simplified to 2D and to a functional form which facilitates the scattering computations.

A 4D PES

The code autoPES[30,31] was used to build a 4D PES for the $CO_2\cdot$Ar dimer, whereby the bond length of the CO_2 monomer unit was fixed at $R_e(CO) = 1.1631$ Å, the equilibrium bond length of the monomer at the frozen-core aug-cc-pVQZ[32] CCSD(T)[33] level of electronic-structure theory. The O–C–O bond angle and the (R, θ, ϕ) coordinates, see Figure 1, were sampled with a weighted randomizing algorithm.[30,31] A total of 1015 grid points were selected in the short-range subspace, for which single-point energies were computed at the frozen-core,

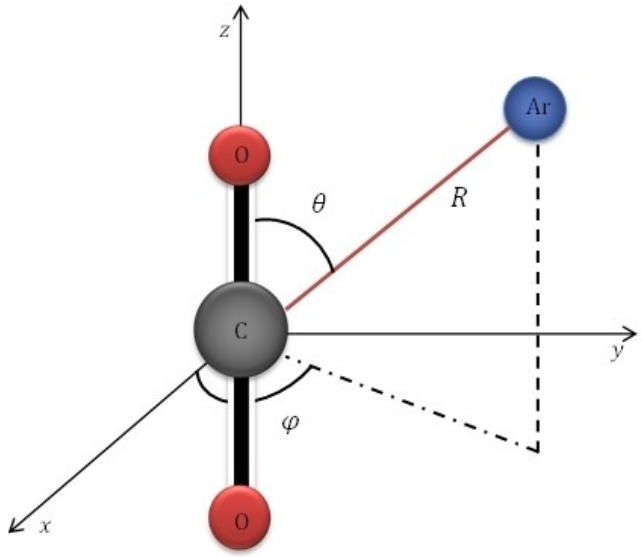

Figure 1. Jacobi-type coordinate system (R, θ, ϕ) describing the position of the Ar atom in the CO_2·Ar dimer with respect to the CO_2 monomer. The origin of the frame coincides with the carbon atom. The distance of the Ar atom from the origin is denoted by R, while θ and ϕ represent the standard spherical coordinates.

counterpoise-corrected[34] CCSD(T) level. In these computations, the aug-cc-pVTZ and aug-cc-pVQZ basis sets were used, extended with midbond functions[35] (this is the default in autoPES). The final interaction energies at short-range configurations were ascertained by extrapolation of the single-point energies to the complete basis set (CBS) limit using the formulas of Ref. [36]. Thus, these electronic energies correspond to the CBS CCSD(T) limit. In the long-range subspace, the interaction energies were obtained, for 4500 grid points, *via* a multipole expansion along the R coordinate, as described in detail in Ref. [37]. The actual electronic-structure computations employed the codes SAPT,[38,39] MOLPRO,[40] and ORCA.[41]

To improve the description of the interactions determined by the intermonomer degrees of freedom, off-atomic (OA) sites were introduced. They were treated as follows: (a) an even number of OA sites, distributed symmetrically around the C atom, were placed on the principal symmetry axis, (b) a common parameter set was employed for the two O atoms, reflecting the permutational symmetry of CO_2 (the same holds for the OA pairs placed at equal distance from the C atom), (c) each OA site was restricted to remain along one of the bonds of CO_2, following the intramonomer bending motion, and (d) the OA positions were optimized simultaneously with the fitting parameters.

As to the accuracy of the fit, the root-mean-square deviation of the computed and the reference energies, for points with negative interaction energy (*i.e.*, those within the potential well), is only 0.02 cm^{-1}. Thus, our fitted 4D PES provides an outstanding representation of the high-level electronic energies.

The PES of the CO_2·Ar vdW dimer is characterized by a T-shaped global minimum of C_{2v} point-group symmetry, where the O–C–O bond angle is 179.98°. The electronic-structure computations performed suggest that the CO_2·Ar complex does not have a (collinear) secondary minimum.

The IM PES

As a next step, we decrease the dimensionality of the 4D PES. In the new PES, the CO_2 molecule is kept linear; therefore, only two intermolecular coordinates, R and θ (see Figure 1) remain active. Based on theoretical considerations,[42,43] we decided to use the following functional form:

$$V(R,\theta;\varphi,\tilde{\chi},\tilde{\theta},\tilde{\varphi}) = \sum_{l\in\{0,2,4,6\}} V_{l,0,l}(R) \sum_{\mu=-l}^{l} \left[D^{l}_{\mu 0}(\tilde{\varphi},\tilde{\theta},\tilde{\chi}) Y_{l\mu}(\theta,\varphi) \right]^{*} \quad (1)$$

where $V_{l,0,l}$ designates a radial function, $D^{l}_{\mu 0}$ is a Wigner-D matrix, $Y_{l\mu}$ means a spherical harmonic function, the asterisk denotes complex conjugation, and $(\tilde{\chi},\tilde{\theta},\tilde{\varphi})$ is formed by three Euler angles specifying the angular orientation of the rigid CO_2 molecule in the CO_2·Ar complex. Due to symmetry reasons, $(\varphi,\tilde{\chi},\tilde{\theta},\tilde{\varphi}) = (0,0,0,0)$ must be employed [hence the parametrical dependence indicated after the semicolon in Eq. (1)].

The radial functions are expanded in this study as follows:

$$V_{l,0,l}(R) = \sum_{p=6}^{12} \frac{a^{(p)}_{l0l}}{R^p}, \quad (2)$$

where the entries of the $(l_1,l_2,l_1+l_2) = (l,0,l)$ triplet are quantum numbers pertaining to the angular-momenta of CO_2 (l_1), Ar (l_2), and CO_2•Ar (l_1+l_2). The $a^{(p)}_{l0l}$ coefficients were adjusted to reproduce the radial form of the 4D PES as accurately as possible. The intermolecular PES defined in Eqs. (1) and (2) is denoted hereafter as 'IM'. The $a^{(p)}_{l0l}$ coefficients of the IM PES are given in Table 1, whereas the radial curves are displayed in Figure 2. Note that the $l=0$ term of Eq. (1) can be reduced to $V_{iso}(R) \equiv V_{0,0,0}(R)$, which is the isotropic part of the IM PES.

Table 1. Fitted values of the $a^{(p)}_{l0l}$ parameters, defined in Eq. (2).

l0l	$p=12$	$p=11$	$p=10$	$p=9$	$p=8$	$p=7$	$p=6$
000	1.36245×10^{8}	-4.01792×10^{8}	4.65304×10^{8}	-2.67921×10^{8}	8.11574×10^{7}	-1.23401×10^{7}	7.18877×10^{5}
202	1.52198×10^{8}	-4.48247×10^{8}	5.19152×10^{8}	-2.99752×10^{8}	9.14623×10^{7}	-1.41006×10^{7}	8.60422×10^{5}
404	6.01341×10^{7}	-1.80662×10^{8}	2.14043×10^{8}	-1.26844×10^{8}	3.98467×10^{7}	-6.32900×10^{6}	3.98236×10^{5}
606	1.44246×10^{7}	-4.47075×10^{7}	5.46672×10^{7}	-3.34269×10^{7}	1.08382×10^{7}	-1.77729×10^{6}	1.15539×10^{5}

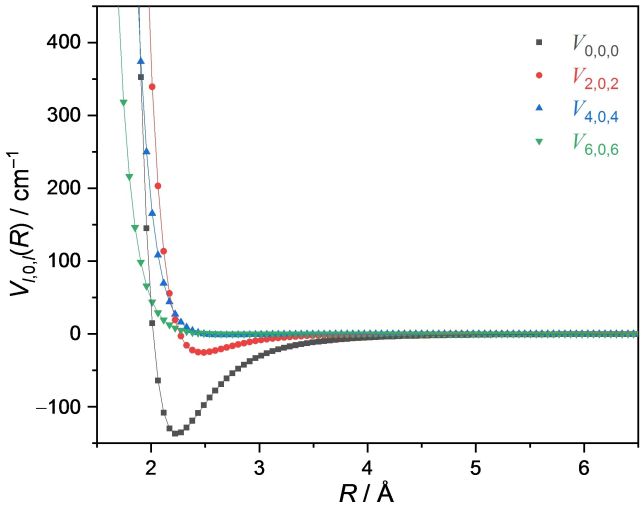

Figure 2. Radial curves of the IM PES obtained for the $CO_2 \cdot Ar$ complex. In this figure, $V_{l,0,l}$ designates the radial function defined in Eq. (2), and R denotes the C–Ar distance. The discrete points correspond to values derived from the 4D PES, whereas the solid lines indicate the fitted analytical curves, showing excellent agreement between the two potential representations.

Computation of Line-Broadening Coefficients and Their Temperature Dependence

Semiclassical calculations of the broadening of rovibrational lines of CO_2 colliding with Ar were carried out within the framework of the modified Robert–Bonamy (MRB) model,[44] utilizing the IM PES and exact time-dependent trajectories for R and θ.[45,46] In this scheme, a radiative transition of CO_2 is assumed to yield an isolated rovibrational line when the radiator, CO_2, is interacting with the perturber, Ar. In what follows, g denotes a general rovibrational state of $CO_2 \cdot Ar$, J_g and V_g symbolize the corresponding rotational and vibrational parent quantum numbers, respectively, and $f \leftarrow i$ indicates a rovibrational transition of $CO_2 \cdot Ar$ from initial state i to final state f.

In the MRB formalism, the half width at half maximum of an $f \leftarrow i$ line, γ_{fi}, is given as[2,47–49]

$$\gamma_{fi} = \frac{n^{Ar}}{2\pi c^{vac}} \int_0^\infty v F(v) \sigma_{fi}(v) dv, \tag{3}$$

where n^{Ar} denotes the number density of the Ar atoms, c^{vac} is the speed of light in vacuum, v designates the velocity norm of the Ar atom approaching CO_2, $F(v)$ designates the Maxwell–Boltzmann velocity distribution, and $\sigma_{fi}(v)$ is the differential cross-section (or diffusion) function[50] representing collisional efficiency. In the complex MRB (CMRB) variant, $\sigma_{fi}(v)$ of Eq. (3) is expressed as[50]

$$\sigma_{fi}^{CMRB}(v) = 2\pi \int_0^\infty b\{1 - \cos \mathrm{Im}[S_1(b,v) + S_{2,fi}(b,v)] \exp[-\mathrm{Re}\, S_{2,fi}(b,v)]\} db, \tag{4}$$

while in the real MRB (RMRB) formalism, $\sigma_{fi}(v)$ of Eq. (3) is[2]

$$\sigma_{fi}^{RMRB}(v) = 2\pi \int_0^\infty b\{1 - \exp[-\mathrm{Re}\, S_{2,fi}(b,v)]\} db, \tag{5}$$

where $S_1(b,v)$ and $S_{2,fi}(b,v)$ are called the first- and second-order interruption functions, respectively. The term $S_1(b,v)$ can be specified as[1]

$$S_1(b,v) = -\frac{3\pi}{8\hbar v b^5} \alpha^{Ar} \left([\mu_i^{CO_2}]^2 - [\mu_f^{CO_2}]^2 + \frac{3}{2} \frac{I^{CO_2} I^{Ar}}{I^{CO_2} + I^{Ar}} [\alpha_f^{CO_2} - \alpha_i^{CO_2}] \right), \tag{6}$$

where $\hbar$ is the reduced Planck constant, $\mu_g^{CO_2}$ and $\alpha_g^{CO_2}$ are the dipole moment and the polarizability of the unperturbed i and f states in CO_2, respectively,[51] α^{Ar} is the polarizability of the Ar atom, and I^{CO_2} and I^{Ar} designate the ionization energies of CO_2 and Ar, respectively. The $\Delta\alpha_{fi}^{CO_2} = \alpha_f^{CO_2} - \alpha_i^{CO_2}$ parameter of Eq. (6) was set to 1.09 Å^3 for all the transitions studied (we arrived at this approximate value after adjusting the CMRB results to the experimental broadenings of Brownsword *et al.*[11]).

For the calculation of the $S_{2,fi}(b,v)$ term of Eqs. (4) and (5) through exact trajectories, one needs to replace the integration variable b with $b = r_c \sqrt{1 - V_{iso}^{\circ}(r_c, v)}$, which implicitly defines the r_c parameter, usually referred to as the distance of the closest approach.[1,2] Furthermore,

$$V_{iso}^{\circ}(r_c, v) = \frac{2V_{iso}(r_c)}{m^{\circ} v^2}\ , \tag{7}$$

where m° is the reduced mass of the $CO_2 \cdot Ar$ dimer. In this case, $\mathrm{Re}\, S_{2,fi}(r_c, v)$ can be formulated as[3]

$$\mathrm{Re}\, S_{2,fi}(r_c, v) = S_{2,i}^{outer}(r_c, v) + S_{2,f}^{outer}(r_c, v) + S_2^{middle}(r_c, v)\ , \tag{8}$$

while $\mathrm{Im}\, S_{2,fi}(r_c, v)$, whose exact form is given in Ref. [3], is obtained here *via* an approximate expression,

$$\mathrm{Im}\, S_{2,fi}(r_c, v) \approx S_{2,f}^{outer}(r_c, v) - S_{2,i}^{outer}(r_c, v). \tag{9}$$

For solvated linear molecules, such as $CO_2 \cdot Ar$, the additive terms of Eq. (8) can be calculated efficiently. Based on the results of Refs. [2] and [48],

$$S_2^{middle}(r_c, v) = -\frac{4r_c^2}{\hbar^2 v^2} \sum_{l \in \{2,4,6\}} \kappa_l F_l^{\circ}(r_c, v), \tag{10a}$$

with

$$\kappa_l = (-1)^{l+J_i+J_f}\frac{\sqrt{M(J_i)M(J_f)}}{M(l)}C^{J_i0}_{J_i0/0}C^{J_f0}_{J_f0/0}W(J_iJ_fJ_iJ_f;1l), \quad (10b)$$

where $M(l)=2l+1$, $C^{J_g0}_{J_g0/0}$ is a Clebsch–Gordan coefficient with $g\in\{i,f\}$, $W(J_iJ_fJ_iJ_f;1l)$ is a Racah coefficient, and $F^{\circ}_l(r_c,v)$ stands for a so-called resonance function. This F°_l function can be formulated as

$$F^{\circ}_l(r_c,v)=\sum_{\mu=-l}^{l}\frac{(l+\mu)!(l-\mu)!}{\left\{2^l\left[\frac{(l+\mu)}{2}\right]!\left[\frac{(l-\mu)}{2}\right]!\right\}^2}\left[\mathrm{I}_{l\mu}(r_c,v)\right]^2, \quad (11)$$

which includes the following integral with respect to the $y=R/r_c$ variable:

$$\mathrm{I}_{l\mu}(r_c,v)=\int_1^{\infty} y\;G(y,r_c,v)\;\cos\beta_\mu(y,r_c,v)\;V_{l,0,l}(r_cy)dy, \quad (12)$$

where

$$G(y,r_c,v)=\left[y^2-1+V^{\circ}_{\mathrm{iso}}(r_c,v)-y^2V^{\circ}_{\mathrm{iso}}(r_cy,v)\right]^{-1/2}, \quad (13)$$

$$\beta_\mu(y,r_c,v)=\frac{\omega_{fi}r_c}{v}A_0(y,r_c,v)+\mu A_2(y,r_c,v)\sqrt{1-V^{\circ}_{\mathrm{iso}}(r_c,v)} \quad (14)$$

$$A_q(y,r_c,v)=\int_1^{y} G(z,r_c,v)z^{1-q}dz, \quad (15)$$

and ω_{fi} is the angular frequency of the $f\leftarrow i$ transition calculated from the effective Hamiltonian parameters of Ref. [52]. As to the $S^{\mathrm{outer}}_{2,g}(r_c,v)$ function of Eqs. (8) and (9) with $g\in\{i,f\}$, one can deduce the expression[2,48]

$$S^{\mathrm{outer}}_{2,g}(r_c,v)=\frac{2r_c^2}{\hbar^2v^2}\sum_{l\in\{2,4,6\}}\frac{1}{M(l)}\sum_{\substack{\breve{g}\\ V_{\breve{g}}=V_g}}\left(C^{J_g0}_{J_g0/0}\right)^2F^{\circ}_l(r_c,v), \quad (16)$$

where the internal sum runs over each $\breve{g}$ state whose vibrational parent is identical to that of g. Note that $C^{J_g0}_{J_g0/0}$ cancels any $\breve{g}$ -related term of Eq. (16) which does not meet the collision selection rule, $(-1)^{\Delta J_{g\breve{g}}}=1$ and $|\Delta J_{g\breve{g}}|\le l$, where $\Delta J_{g\breve{g}}=J_g-J_{\breve{g}}$.

To provide an improved representation for the temperature dependence of the $\gamma\equiv\gamma_{fi}$ parameters, Gamache and Vispoel introduced a so-called multiple power-law (MPL) model:[53]

$$\gamma(\Theta)=\sum_{k=1}^{P}c_k\Theta^{n_k}, \quad (17)$$

where $\Theta=T^{\mathrm{ref}}/T$ is the relative temperature with respect to a T^{ref} reference temperature, P is the number of power-law (PL) terms, and c_k and n_k designate the prefactor and the temperature exponent of the kth PL term, respectively. The MPL scheme of Eq. (17) can be viewed as an extension of the standard PL form, $\gamma(\Theta)=c\Theta^n$.[24] The T^{ref} parameter is set to 296 K in this study.

Following the protocol of Ref. [53], an attempt was made to employ the double-power-law (DPL) model,

$$\gamma(\Theta)=c_1\Theta^{n_1}+c_2\Theta^{n_2}, \quad (18)$$

for the description of the broadening coefficients over a set of temperatures. However, for the present case, strong correlation was found between n_1 and n_2 of Eq. (18), making DPL inapplicable for all the transitions considered.

To overcome this difficulty, an alternative model is used, obtained by modifying Eq. (17) as follows:

$$\gamma(\Theta)=\sum_{k=1}^{P}c_k\Phi_k(\Theta), \quad (19)$$

where $\Phi_k(\Theta)>0$ is a suitable function with $\Phi_k(1)=1$. Assuming the existence of the required derivatives, the positive $\Phi_k(\Theta)$ function can be approximated as a truncated logarithmic power series,

$$\log\Phi_k(\Theta)=n_k\log\Theta+n'_k\log^2\Theta+n''_k\log^3\Theta+\dots. \quad (20)$$

Eq. (20) leads to a generalized multiple-power-law (gMPL) model,

$$\gamma(\Theta)=\sum_{k=1}^{N}c_k\Theta^{n_k+n'_k\log\Theta+n''_k\log^2\Theta+\dots}. \quad (21)$$

In this study the γ values do not change sign over a wide temperature range of 80-800 K (*vide infra*); thus, Eq. (21) could be reduced to a 4-parameter model, abbreviated as GPL3:

$$\gamma^{\mathrm{GPL3}}(\Theta)=c\Theta^{n+n'\log\Theta+n''\log^2\Theta}. \quad (22)$$

Results and Discussion

Following the procedure outlined in the previous section, Ar-broadening coefficients have been determined for lines of certain bands, 10001←00011, 01101←00001, 00011←00001, and 00031←00001, of CO_2 at multiple temperature values. In what follows, the computed results are compared to previous literature values.

Pressure-Broadening Coefficients for Lines in the 00011← 00001 Band

First, let us analyze the broadenings of lines in the 00011← 00001 band of CO_2, studied extensively in the literature.[6,11–13,20] Let the temperature be 296 K. Figure 3 illustrates the computed Ar-broadening coefficients against the absolute value of the quantum number m (note that $m=-J$ in the P branch and $m=J+1$ in the R branch). This figure also presents the latest experimental results,[6,11–13] indicating reasonable agreement across the full range of $|m|$ values. Our computational results

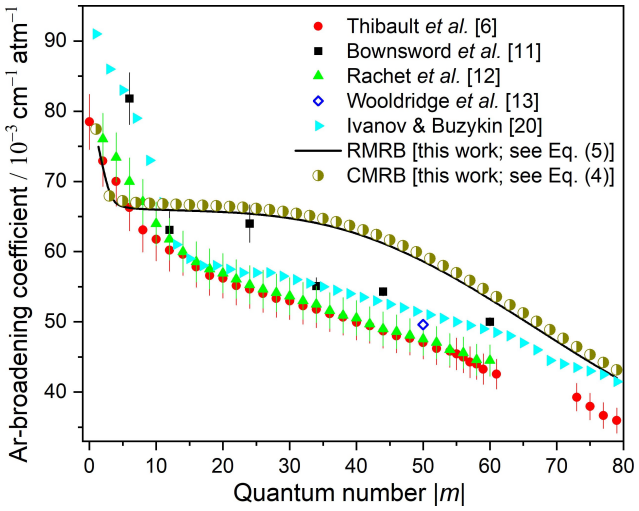

Figure 3. Comparison of Ar-broadening coefficients, obtained at 296 K, for lines in the 00011←00001 band of CO_2. RMRB and CMRB correspond to this work.

are also compared to those of Ivanov and Buzykin,[20] which rely on exact trajectories but do not take into account the Maxwell–Boltzmann velocity distribution. As clear from Figure 3, our CMRB estimates agree well, but are slightly higher than their RMRB counterparts.

To test the reliability of the semiclassical protocol employed here, the line widths of the 00011←00001 band have also been computed at a low temperature, $T=160$ K. The numerical data obtained for $0\leq|m|\leq80$ are illustrated in Figure 4. Clearly, our CMRB and RMRB estimates agree well with each other. They are compared to those observed by Brownsword *et al.*[11] and calculated by Buldyreva *et al.*,[7] as well. Except for one case, our predictions lie fairly close to those of Ref. [11], while the values of Ref. [7] are systematically lower. These deviations can be rationalized by noting that the computations of Ref. [7] relied

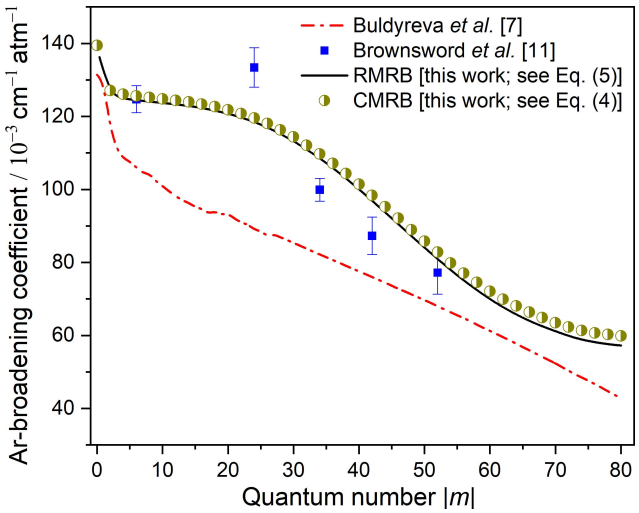

Figure 4. Comparison of Ar-broadening coefficients, obtained at 160 K, for lines in the 00011←00001 band of CO_2. RMRB and CMRB correspond to this work.

on (a) average velocities rather than those integrated over the Maxwell–Boltzmann velocity distribution, and (b) an earlier CO_2·Ar PES,[21] which is less accurate than the one developed in this study. Thus, the discrepancies between the two datasets are about as large as one would expect. For a few transitions, our computations were repeated at a high temperature, 765 K, and these test results also match well their literature counterparts.[6,20]

Pressure-Broadening Coefficients for Lines in the 10001←00011 Band

Table 2 reports computed Ar-broadening coefficients obtained in this work at $T=300$ K for lines in the 10001←00011 band of CO_2. The corresponding experimental values determined by Boulet *et al.*,[44] measured using a stabilized laser source, are also provided. To appreciate the quality of the present computations, Table 2 also contains unsigned percent deviations (UPD), specified as

$$\mathrm{UPD}^{\langle E_1,E_2\rangle}=100\,\left|\gamma^{\langle E_1\rangle}-\gamma^{\langle E_2\rangle}\right|/\gamma^{\langle E_1\rangle}, \tag{23}$$

where $\gamma^{\langle E_1\rangle}$ and $\gamma^{\langle E_2\rangle}$ are two distinct estimates for the broadening parameter of the same transition.

From R(3) to R(39), our predictions exhibit an overall decrease and closely mimic their experimental counterparts, especially for low J values. Similarly, the computed broadenings of the P branch are also characterized with a decreasing trend for $4\leq J\leq40$ and match the low-J measurement values. The average UPD from the observed data is about 10% for both the CMRB and RMRB models, less than the mean experimental accuracy, 11.2%. The UPDs between the CMRB and RMRB predictions are small, only 1.3% on average.

Pressure-Broadening Coefficients for Lines in the 00031←00001 Band

Table 3 lists the computed Ar-broadening coefficients for the 00031←00001 band of CO_2, together with the measured values of Thibault and co-workers,[5] both obtained at room temperature. From R(3) to R(13), our computed data follow closely the monotonous decrease in the observed broadenings, with mean UPDs of 5.4% and 6.3% for the CMRB and RMRB models, respectively. A similar pattern can be seen for the P branch, where our computed estimates decrease as J increases, while the measured broadening parameters show moderate fluctuations. In this case, the average UPDs, with respect to the experimental values,[5] are 13.1% and 12.4% for the CMRB and RMRB models, respectively. As seen in the previous subsection, the typical UPDs between the CMRB and RMRB broadenings are on the order of 1% for both branches. This good overall agreement supports the high quality of the IM PES, as well as the adequacy of the methodology employed.

Table 2. Experimental and computed Ar-broadening coefficients, in 10^{-3} cm^{-1} atm^{-1}, determined at 300 K for lines in the 10001←00011 band of CO_2. The lines are characterized by a branch symbol, P/R, and the *J* value of the initial state, given in parentheses. UPD (unsigned percent deviation) is defined in Eq. (23).

		Calc. (this work)		$UPD^{\langle Calc., Expt.\rangle}$	
Line	Expt.[4]	CMRB	RMRB	CMRB	RMRB
R(3)	67±10	66.41	65.56	0.9	2.2
R(5)	69±8	66.04	65.19	4.5	5.8
R(7)	77±9	65.91	65.06	16.8	18.4
R(9)	73±8	65.83	64.98	10.9	12.3
R(11)	65±6	65.76	64.92	1.2	0.1
R(13)	64±9	65.71	64.87	2.6	1.3
R(15)	62±6	65.64	64.81	5.5	4.3
R(17)	60±6	65.56	64.74	8.5	7.3
R(19)	58±6	65.47	64.65	11.4	10.3
R(21)	60±9	65.38	64.57	8.2	7.1
R(23)	58±8	65.20	64.39	11.0	9.9
R(25)	59±5	65.06	64.26	9.3	8.2
R(27)	56±6	64.87	64.07	13.7	12.6
R(29)	54±5	64.62	63.82	16.4	15.4
R(31)	57±7	64.31	63.52	11.4	10.3
R(33)	52±6	63.97	63.18	18.7	17.7
R(35)	53±5	63.58	62.78	16.6	15.6
R(37)	51±5	63.09	62.29	19.2	18.1
R(39)	49±5	62.54	61.74	21.7	20.6
P(4)	65±7	66.41	65.56	2.1	0.9
P(6)	70±9	66.04	65.19	6.0	7.4
P(8)	69±8	65.91	65.06	4.7	6.1
P(10)	64±9	65.82	64.98	2.8	1.5
P(12)	62±5	65.76	64.92	5.7	4.5
P(14)	60±7	65.71	64.87	8.7	7.5
P(16)	60±9	65.64	64.81	8.6	7.4
P(18)	59±4	65.57	64.74	10.0	8.9
P(20)	62±7	65.47	64.65	5.3	4.1
P(22)	59±4	65.39	64.58	9.8	8.6
P(24)	57±6	65.20	64.39	12.6	11.5
P(26)	61±5	65.06	64.26	6.2	5.1
P(28)	54±6	64.87	64.07	16.8	15.7
P(30)	52±6	64.62	63.82	19.5	18.5
P(32)	53±7	64.32	63.52	17.6	16.6
P(34)	53±5	63.99	63.19	17.2	16.1
P(36)	54±7	63.58	62.78	15.1	14.0
P(38)	49±6	63.09	62.29	22.3	21.3
P(40)	52±7	62.54	61.74	16.9	15.8

Table 3. Experimental and theoretical Ar-broadening coefficients, in 10^{-3} cm^{-1} atm^{-1}, determined for the 00031←00001 band of CO_2 at 296 K. The assignment of a specific line contains its branch symbol, P/R, and the *J* value of its initial state in parentheses. UPD (unsigned percent deviation) is defined in Eq. (23).

		Calc. (this work)		$UPD^{\langle Calc., Expt.\rangle}$	
Line	Expt.[5]	CMRB	RMRB	CMRB	RMRB
R(3)	76.55	67.43	66.57	13.5	15.0
R(5)	71.70	67.07	66.21	6.9	8.3
R(7)	70.80	66.92	66.06	5.8	7.2
R(9)	68.35	66.84	65.98	2.3	3.6
R(11)	67.05	66.77	65.92	0.4	1.7
R(13)	64.30	66.71	65.87	3.6	2.4
P(2)	81.50	69.41	68.59	17.4	18.8
P(4)	73.50	67.44	66.58	9.0	10.4
P(6)	70.45	67.08	66.22	5.0	6.4
P(8)	65.55	66.93	66.07	2.1	0.8
P(10)	62.25	66.84	65.99	6.9	5.7
P(12)	62.40	66.78	65.93	6.6	5.4
P(14)	60.85	66.71	65.87	8.8	7.6
P(16)	60.35	66.65	65.81	9.5	8.3
P(18)	58.15	66.57	65.74	12.6	11.5
P(20)	56.50	66.48	65.65	15.0	13.9
P(22)	59.40	66.37	65.55	10.5	9.4
P(24)	57.20	66.25	65.43	13.7	12.6
P(26)	57.70	66.06	65.25	12.7	11.6
P(28)	55.75	65.86	65.05	15.4	14.3
P(30)	53.85	65.61	64.80	17.9	16.9
P(32)	51.40	65.31	64.50	21.3	20.3
P(34)	48.70	64.96	64.15	25.0	24.1
P(36)	47.70	64.52	63.72	26.1	25.1

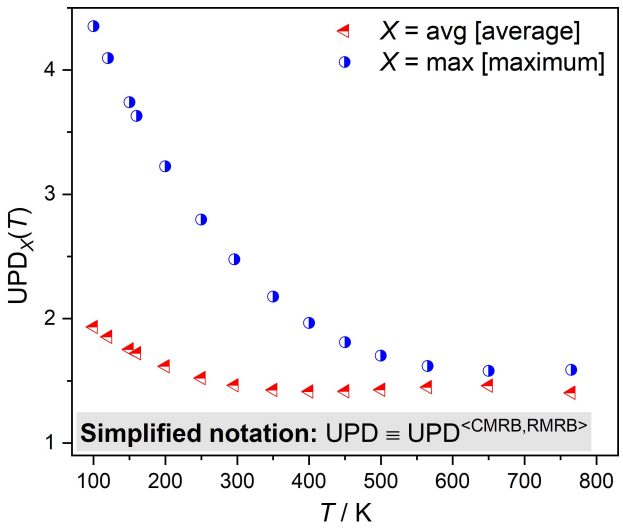

Figure 5. Temperature-dependent deviations of the CMRB and RMRB results in the 00011←00001 band. The $UPD_X(T)$ values correspond to the average (X = avg) and the maximum (X = max) of the UPDs obtained for 41 transitions at absolute temperature *T*.

Pressure-Broadening Coefficients for Lines in the 01101←00001 Band

Due to the importance of the 01101←00001 band during the investigation of the greenhouse effect, our study has been

Table 4. Temperature-dependent models for the Ar-broadenings of selected lines in the 01101←00001 band. The broadening values have been computed *via* the RMRB model in the 80–800 K temperature range. Columns 2–4 show the root mean-square deviations (RMSD) of the PL, DPL, and GPL3 models, introduced in Eq. (17), Eq. (18), and Eq. (22), respectively. The GPL3 parameters, along with the standard 1σ uncertainties of the last digits in parentheses, are placed in the last four columns. The asterisked values are fixed to zero in the GPL3 model.

	unit: 10^{-3} cm^{-1} atm^{-1}				unit: dimensionless		
Line	RMSD(PL)	RMSD(DPL)	RMSD(GPL3)	*c*	*n*	*n′*	*n″*
R(0)	5.18	1.34	0.59	76.4(2)	1.044(4)	−0.137(4)	0.0*
R(2)	4.71	0.99	0.60	67.1(3)	1.095(5)	−0.121(9)	−0.016(7)
R(4)	4.76	0.97	0.59	66.4(3)	1.100(5)	−0.121(9)	−0.018(7)
R(6)	4.84	0.97	0.58	66.2(3)	1.101(5)	−0.122(9)	−0.019(7)
R(8)	4.96	0.94	0.55	66.0(2)	1.101(5)	−0.123(8)	−0.022(6)
R(10)	5.04	1.00	0.58	66.0(3)	1.099(5)	−0.127(9)	−0.021(7)
R(12)	5.20	1.00	0.57	65.9(2)	1.098(5)	−0.130(9)	−0.024(6)
R(14)	5.41	1.00	0.56	65.9(2)	1.097(5)	−0.132(9)	−0.028(6)
R(16)	5.68	0.98	0.53	65.8(2)	1.097(5)	−0.135(8)	−0.033(6)
R(18)	6.00	1.03	0.55	65.6(2)	1.097(5)	−0.140(9)	−0.038(6)
R(20)	6.38	1.07	0.47	65.5(2)	1.096(4)	−0.152(7)	−0.040(6)
R(22)	6.73	1.09	0.45	65.4(2)	1.092(4)	−0.158(7)	−0.046(5)
R(24)	7.05	1.23	0.51	65.3(2)	1.084(5)	−0.169(8)	−0.049(6)
R(26)	7.34	1.33	0.52	65.1(2)	1.075(5)	−0.179(8)	−0.051(6)
R(28)	7.49	1.61	0.69	64.9(3)	1.058(7)	−0.20(1)	−0.045(8)
R(30)	7.52	1.96	0.83	64.8(4)	1.036(8)	−0.22(1)	−0.03(1)
R(32)	7.54	2.09	0.93	64.9(3)	1.009(8)	−0.258(8)	0.0*
R(34)	7.58	2.36	0.91	64.2(3)	0.993(8)	−0.264(8)	0.0*
R(36)	7.48	2.59	1.02	63.5(3)	0.972(9)	−0.265(9)	0.0*
R(38)	7.32	2.66	1.16	62.6(4)	0.95(1)	−0.26(1)	0.0*
R(40)	7.09	2.48	1.29	62.4(6)	0.91(1)	−0.30(2)	0.04(2)
R(42)	6.72	2.33	1.53	61.7(7)	0.87(2)	−0.32(3)	0.07(2)
R(44)	6.29	2.32	1.76	60.9(8)	0.82(2)	−0.33(3)	0.10(3)
R(46)	5.86	2.54	1.96	60.0(9)	0.78(2)	−0.35(4)	0.14(3)
R(48)	5.46	3.02	2.17	59(1)	0.72(2)	−0.36(4)	0.19(3)
R(50)	5.22	3.49	2.27	58(1)	0.68(3)	−0.37(4)	0.23(3)
R(52)	5.03	3.94	2.28	57(1)	0.63(3)	−0.36(4)	0.26(3)
R(54)	4.99	4.38	2.22	56(1)	0.60(3)	−0.35(4)	0.29(3)
R(56)	5.11	4.25	2.11	54.2(9)	0.56(3)	−0.34(4)	0.32(3)
R(58)	5.37	3.92	1.97	52.8(9)	0.53(2)	−0.32(4)	0.34(3)
R(60)	5.73	3.69	1.77	51.5(8)	0.51(2)	−0.30(3)	0.36(3)
R(62)	6.18	3.46	1.61	50.1(7)	0.49(2)	−0.27(3)	0.38(3)
R(64)	6.68	3.27	1.47	48.8(6)	0.47(2)	−0.24(3)	0.38(2)
R(66)	7.23	3.09	1.34	47.4(6)	0.47(2)	−0.20(3)	0.39(2)
R(68)	7.62	2.99	1.32	46.1(6)	0.47(2)	−0.16(3)	0.38(2)
R(70)	7.97	2.94	1.45	44.7(6)	0.48(2)	−0.12(3)	0.36(2)
R(72)	8.33	2.92	1.57	43.5(7)	0.49(2)	−0.08(3)	0.35(2)
R(74)	8.56	2.83	1.71	41.8(5)	0.51(2)	0.0*	0.30(1)
R(76)	8.76	2.79	1.88	41.3(5)	0.53(2)	0.0*	0.30(1)
R(78)	8.90	2.73	2.12	40.9(6)	0.55(3)	0.0*	0.30(2)
R(80)	9.04	2.72	2.40	40.5(7)	0.58(3)	0.0*	0.31(2)

extended to this band, as well. For the 01101←00001 band, no experimental data are accessible for comparison, but similar accuracy is expected here as for the other bands discussed above, that is, a couple of percent in relative terms.

To compare the broadening data of the 01101←00001 and 00011←00001 bands, our computations have been carried out for 41 transitions within the two bands. The broadening coefficients, obtained at 22 temperature values in the range of 80–800 K with the RMRB model, are given in the Supplementary Material (Tables S1 and S2). These results indicate that the differences between the broadening coefficients of the 01101←00001 and 00011←00001 bands are small [the largest deviation is 7×10^{-4} $cm^{-1}atm^{-1}$ at 80 K for R(80)]. As obvious from Figure 5, the deviations between the CMRB- and RMRB-based estimates also decrease with the increase of the temperature, remaining below 5% in the region studied.

For the 41 lines analyzed in the 01101←00001 band of CO_2, three distinct models have been utilized to describe the temperature dependence of the broadening coefficients. The results of our fits yielded with the PL [Eq. (17)], DPL [Eq. (18)], and GPL3 [Eq. (22)] models are summarized in Table 4. As Table 4 reveals, the fitting errors are the smallest for the GPL3 model. Note that the n_1 and n_2 parameters of the DPL model became strongly correlated, producing unacceptably large uncertainties for these exponents in all cases. For a few transitions, there were parameters with high uncertainties in the GPL3 model, as well, but they could be eliminated by fixing them to zero, which did not cause a significant increase in the fitting residuals. Nevertheless, this is not the case for the DPL model, where none of the four parameters could be frozen without a notable increase in the fitting errors.

To validate the GPL3 model results shown in Table 4, the same fits have been carried out for the broadenings of the 00011←00001 band, as well. These fits reveal no significant differences among the models of the two bands. Since changes in the GPL3 parameters remain within the calculated uncertainties, the GPL3 model of Table 4 can be applied for lines in the 00011←00001 band, as well. For the R(50) transition, GPL3 yields $n=0.68$, which is in good accord with $n=0.61$,[13] a value derived from experimental broadenings in the 00011←00001 band *via* the standard PL model. Furthermore, the agreement is also good with another experimental/empirical estimate, $n=0.88\pm0.18$, reported for $J\leq40$ in Ref. [11].

Conclusions

With the goal of determining temperature-dependent line broadenings for the CO_2 molecule perturbed by an Ar atom, a high-quality intermonomer potential energy surface was developed for the CO_2·Ar van der Waals complex. The semiclassical method used for the computation of the broadenings is built upon the modified Robert–Bonamy (MRB) formalism and the exact trajectory model. Within the MRB model we consider both the real and the complex terms.

For the CO_2·Ar model and the bands chosen, differences between the results obtained with the real and imaginary formalisms are rather small. As expected, our results show improvement over previous determinations[7] of line broadening parameters, perhaps due partially to the high quality of the PES we use.

Computations of the broadening parameters were performed at 22 temperature values in the 80–800 K range, for the 00011←00001 and 01101←00001 bands, whereas for the 10001←00011 and 00031←00001 bands they were carried out at 300 and 296 K, respectively. The 00011←00001 band of the CO_2 molecule has been subjected to numerous studies when CO_2 interacts with Ar, allowing the validation of our computed Ar-broadening coefficients. For the first time, this study provides very useful Ar-broadening coefficients and temperature parameters for lines in the 01101←00001 band.

Beyond the standard power-law (PL)[24] and the multiple PL[53] models, a new functional form, called here the generalized PL (GPL) model, was utilized to describe the temperature dependence of the broadening values of lines in the 00011←00001 and 01101←00001 bands. Using at most four parameters in the fits, the GPL model delivers the best representation for these broadening coefficients as a function of temperature. Although the GPL scheme was tested only on CO_2·Ar, it might be useful for other systems, as well. This would require further investigations.

Notes: The authors declare no competing financial interest.

Acknowledgements

The authors extend their appreciation to the Researchers Supporting Project (RSPD2023R808) of King Saud University, Riyadh, Saudi Arabia. The work performed in Budapest received support from NKFIH (grant no. K138233 and PD145972), the HUN-REN Hungarian Research Network, and the grant VEKOP-2.3.2-16-2017-00014. This publication supports research performed within the COST Action CA21101 "Confined molecular systems: from a new generation of materials to the stars" (COSY), funded by the European Cooperation in Science and Technology (COST) and the MSCA Doctoral Network PHYMOL, "Physics, Accuracy and Machine Learning: Towards the Next Generation of Molecular Potentials".

Conflict of Interests

The authors declare no conflict of interest.

Data Availability Statement

The data that support the findings of this study are available from the corresponding author upon reasonable request.

Keywords: temperature-dependent line broadening parameters · Ar-broadened CO_2 rovibrational transitions · interaction potential energy surface · modified Robert–Bonamy approach · generalized power-law model

[1] J. Buldyreva, N. Lavrentieva, V. Starikov, *Collisional Line Broadening and Shifting of Atmospheric Gases*, World Scientific, Imperial College Press, London, **2010**.
[2] J. Buldyreva, M. Guinet, S. Eliet, F. Hindle, G. Mouret, R. Bocquet, A. Cuisset, *Phys. Chem. Chem. Phys.* **2011**, *13*, 20326–20334.
[3] D. Robert, J. Bonamy, *J. Phys. France* **1979**, *40*, 923–943.
[4] C. Boulet, P. Isnard, E. Arie, *J. Quant. Spcctrosc. Rodiat. Transf.* **1974**, *14*, 637–649.
[5] F. Thibault, J. Boissoles, R. Le Doucen, J. P. Bouanich, P. Arcas, C. Boulet, *J. Chem. Phys.* **1992**, *96*, 4945–4953.
[6] F. Thibault, B. Calil, J. Buldyreva, M. Chrysos, J.-M. Hartmann, J.-P. Bouanich, *Phys. Chem. Chem. Phys.* **2001**, *3*, 3924–3933.
[7] J. Buldyreva, M. Chrysos, *J. Chem. Phys.* **2001**, *115*, 7436–7441.
[8] E. W. Smith, M. Giraud, J. Couper, *J. Chem. Phys.* **1976**, *65*, 1256–1267.
[9] R. Goldflam, S. Green, D. J. Kouri, *J. Chem. Phys.* **1977**, *67*, 4149–4161.
[10] R. T. Pack, *J. Chem. Phys.* **1979**, *70*, 3424–3433.
[11] R. A. Brownsword, J. S. Salh, I. W. M. Smith, *J. Chem. Soc. Faraday Trans.* **1995**, *91*, 191–195.
[12] F. Rachet, M. Margottin-Maclou, A. Henry, A. Valentin, *J. Mol. Spectrosc.* **1996**, *175*, 315–326.
[13] M. S. Wooldridge, R. K. Hanson, C. T. Bowman, *J. Quant. Spectrosc. Radiat. Transf.* **1997**, *57*, 425–434.
[14] R. R. Gamache, J. Lamouroux, *J. Quant. Spectrosc. Radiat. Transf.* **2013**, *117*, 93–103.
[15] D. D. Lee, F. A. Bendana, A. P. Nair, D. I. Pineda, R. M. Spearrin, *J. Quant. Spectrosc. Radiat. Transf.* **2020**, *253*, 107135.
[16] R. K. Cole, H. Tran, N. Hoghooghi, G. B. Rieker, *J. Quant. Spectrosc. Radiat. Transf.* **2023**, *297*, 108488.
[17] M. Gu, S. Wang, G. Wang, Q. Wang, X. Liu, F. Qi, C. S. Goldenstein, *Appl. Phys. B* **2022**, *128*, 131.
[18] D. Chen, L. Shi, P. Xu, R. Wang, C. Zhang, *J. Mol. Spectrosc.* **2021**, *377*, 111429.
[19] S. V. Ivanov, O. G. Buzykin, *J. Quant. Spectrosc. Radiat. Transf.* **2013**, *119*, 84–94.
[20] S. V. Ivanov, O. G. Buzykin, *J. Quant. Spectrosc. Radiat. Transf.* **2016**, *185*, 48–57.
[21] G. A. Parker, R. L. Snow, R. T. Pack, *J. Chem. Phys.* **1976**, *64*, 1668–1678.
[22] K. I. Arshinov, M. K. Arshinov, V. V. Nevdakh, *Opt. Spectrosc.* **2012**, *112*, 844–849.
[23] K. I. Arshinov, O. N. Krapivnaya, V. V. Nevdakh, S. R. Syrtsov, V. N. Shut, *Opt. Spectrosc.* **2018**, *125*, 1–4.
[24] K. I. Arshinov, O. N. Krapivnaya, V. V. Nevdakh, V. N. Shut, *Atmos. Ocean. Opt.* **2020**, *33*, 229–237.
[25] R. L. Armstrong, *Appl. Opt.* **1982**, *21*, 2141–2145.
[26] J. R. Aronson, P. C. von Thüna, J. F. Butler, *Appl. Opt.* **1975**, *14*, 1120–1127.
[27] W. G. Planet, G. L. Tettemer, J. S. Knoll, *J. Quant. Spectrosc. Radiat. Transf.* **1978**, *20*, 547–556.
[28] W. G. Planet, G. L. Tettemer, *J. Quant. Spectrosc. Radiat. Transf.* **1979**, *22*, 345–354.
[29] G. L. Tettemer, W. G. Planet, *J. Quant. Spectrosc. Radiat. Transf.* **1980**, *24*, 343–345.
[30] M. P. Metz, K. Piszczatowski, K. Szalewicz, *J. Chem. Theory Comput.* **2016**, *12*, 5895–5919.
[31] M. P. Metz, K. Szalewicz, *J. Chem. Theory Comput.* **2020**, *16*, 2317–2339.
[32] T. H. Dunning Jr., *J. Chem. Phys.* **1989**, *90*, 1007–1023.
[33] K. Raghavachari, G. W. Trucks, J. A. People, M. Head-Gordon, *Chem. Phys. Lett.* **1989**, *157*, 479–483.
[34] S. F. Boys, F. Bernardi, *Mol. Phys.* **1970**, *19*, 553–566.
[35] O. Akin-Ojo, R. Bukowski, K. Szalewicz, *J. Chem. Phys.* **2003**, *119*, 8379–8396.
[36] T. Helgaker, W. Klopper, H. Koch, J. Noga, *J. Chem. Phys.* **1997**, *106*, 9639–9646.
[37] B. Jeziorski, R. Moszynski, K. Szalewicz, *Chem. Rev.* **1994**, *94*, 1887–1930.
[38] R. Bukowski, W. Cencek, P. Jankowski, M. Jeziorska, B. Jeziorski, T. Korona, S. A. Kucharski, V. F. Lotrich, A. J. Misquitta, R. Moszynski, K. Patkowski, R. Podeszwa, S. Rybak, K. Szalewicz, H. L. Williams, R. J. Wheatley, P. E. S. Wormer, P. S. Zuchowski, SAPT2016: An ab initio program for symmetry-adapted perturbation theory, **2016**.
[39] J. Garcia, R. Podeszwa, K. Szalewicz, *J. Chem. Phys.* **2020**, *152*, 184109.
[40] https://www.molpro.net.
[41] F. Neese, F. Wennmohs, U. Becker, C. Riplinger, *J. Chem. Phys.* **2020**, *152*, 224108.
[42] T. Gabard, J. P. Champion, *J. Quant. Spectrosc. Radiat. Transf.* **1994**, *52*, 303–317.
[43] R. Lynch, R. R. Gamache, S. P. Neshyba, *J. Quant. Spectrosc. Radiat. Transf.* **1998**, *59*, 595–613.
[44] Q. Ma, R. H. Tipping, C. Boulet, *J. Quant. Spectrosc. Radiat. Transf.* **2007**, *103*, 588–596.
[45] A. D. Bykov, N. N. Lavrentieva, L. N. Sinitsa, *Atmos. Oceanic. Opt.* **1992**, *5*, 587.
[46] A. D. Bykov, N. N. Lavrentieva, L. N. Sinitsa, *Atmos. Oceanic. Opt.* **1992**, *5*, 728.
[47] J. Salem, J. P. Bouanich, J. Walrand, H. Aroui, G. Blanquet, *J. Mol. Spectrosc.* **2005**, *232*, 247–254.
[48] J. Salem, M. Salem, M. Dhib, R. Ben Younes, H. Aroui, M. Hochlaf, *Mol. Phys.* **2022**, *120*, e2130110.
[49] J. Salem, A. Badri, M. Salem, M. Mogren Al-Mogren, M. Hochlaf, *Phys. Chem. Chem. Phys.* **2023**, *25*, 11237.
[50] R. R. Gamache, J. Lamouroux, A. L. Laraia, J.-M. Hartmann, C. Boulet, *J. Quant. Spectrosc. Radiat. Transf.* **2012**, *113*, 976–990.
[51] T. Hirano, U. Nagashima, P. Jensen, H. Lid, *J. Mol. Spectrosc.* **2019**, *362*, 29–36.
[52] L. S. Rothman, R. L. Hawkins, R. B. Wattson, R. R. Gamache, *J. Quant. Spectrosc. Radiat. Transf.* **1992**, *48*, 537–566.
[53] R. R. Gamache, B. Vispoel, *J. Quant. Spectrosc. Radiat. Transf.* **2018**, *217*, 440–452.

Manuscript received: July 1, 2023
Revised manuscript received: October 28, 2023
Accepted manuscript online: November 2, 2023
Version of record online: November 2, 2023